A Passive All-Optical Device for 2R Regeneration Based on the Cascade of Two High-Speed Saturable Absorbers

Hoang Trung Nguyen, Coraline Fortier, Julien Fatome, Guy Aubin, and Jean-Louis Oudar

***Abstract*—We discuss the design and realization of a passive all-optical device for 2R regeneration based on a dual-stage of high-speed microcavity saturable absorbers, one for noise reduction of digital zeros (SA-0), and the other for noise reduction of digital ones (SA-1). The numerical and experimental results showed that by using a simple combination of SA-0 and SA-1 devices, one can obtain an intensity transfer function with a large extinction ratio improvement of low power levels and a strongly nonlinear response reducing the noise of high power levels. The amplitude and phase characterization of a 40-GHz signal transmitted by this device, obtained by frequency-resolved optical gating measurements, reveals the intensity-dependant pulse-compression effect and the low chirp introduced by this device.**

***Index Terms*—All-optical switching gates, asymmetric Fabry–Perot devices, high-speed optical techniques, nonlinear optics, optical regeneration, optical saturable absorption, semiconductor quantum well (QW).**

I. Introduction

HIGH-SPEED networks will need to use ultrafast optical devices with extremely low chirp. Optical-communication systems are subject to several sources of signal degradation. Some impairments, such as signal attenuation and dispersion, can be cured by amplification and dispersion compensation. However, the random noise from amplifiers requires more general methods of signal restoration. Ultrafast all-optical reshaping regeneration (2R regeneration) is necessary for high-speed networks to improve the SNR through extinction ratio (ER) improvement and noise redistribution [1]. These improvements can be achieved with devices, which have a nonlinear transfer function (output power as a function of input power). This nonlinear response enables to increase the discrimination between logical ones and zeros [1]. Several schemes of 2R regenerator have been proposed [2]–[8]. Among these, the simple scheme of all-optical 2R regenerator based on saturable absorbers (SAs) in optical microcavity is particularly attractive, owing to its simplicity and its fully passive operation mode (no Peltier cooler, no bias voltage) [9]. Recent experiments using high-repetition-rate signals showed that with the benefit of quantum wells (QWs) having an ultrafast carrier recombination rate [10], [11], SA microcavity devices are very promising devices for 2R regeneration at 160 Gb/s [12], [13].

Nevertheless, SAs actually have only been used to achieve an ER improvement without impacting the noise in bit-1 level. In order to perform a complete regeneration, SAs have typically been used in combination with other devices that can provide the level stabilization at the bit time scale. While the recent advances in fiber-SA-based gates or SOA-SA-based gates have allowed to demonstrate attractive characteristics, they typically suffer from limited performance concerning the polarization dependence, the induced chirp, the requirement of strong input power [14], [15] and insufficient speed [15], [16]. Moreover, they are not adequate for wavelength-division multiplexing (WDM) applications. The recent investigation of a SA-based microcavity passive all-optical device, which can provide an amplitude stabilization, and thus, a noise reduction of bit-1 levels, allows a solution for passive all-optical regeneration based on SAs [17], [18]. The potential advantage of this approach is to make a complete passive all-optical high-bit-rate 2R regeneration relying upon a single technology. SA-based microcavities, on the other hand, offer a number of unique advantages, including polarization-independent operation, low insertion loss, high contrast ratio, and high speed and compatibility with WDM applications [19].

In this paper, we propose and study experimentally passive all-optical-device-based SAs that could be used for 2R regeneration. We demonstrate that some important properties of the power transfer function, such as a large attainable ER and a strong nonlinearity, can be achieved by using a simple combination of two SA devices named SA-0 and SA-1. The SA-0 is used to improve the ER, while the SA-1 provides a significant stabilization at high amplitude levels, representing the logical ones. Furthermore, a 40-GHz signal processed by the dual-stage $(\mathrm{SA}-0+\mathrm{SA}-1)$ device has been characterized in intensity and phase by frequency-resolved optical gating (FROG) measurements [20].

II. Review of Device Design

The nonlinearity of SA-based devices is achieved by the modulation of carrier density in active layer. In order to obtain good saturation characteristics, InP-based multi-QWs,

Manuscript received September 17, 2010; revised December 02, 2010; accepted January 18, 2011. Date of publication February 22, 2011; date of current version April 22, 2011. This work was supported in part by the French National Research Agency (ANR—FUTUR).

H. T. Nguyen, G. Aubin, and J.-L. Oudar are with the Laboratory for Photonics and Nanostructures, Centre National de la Recherche Scientifique UPR20, 91460 Marcoussis, France (e-mail: hoang-trung.nguyen@lpn.cnrs.fr).

C. Fortier and J. Fatome are with Laboratoire Interdisciplinaire Carnot de Bourgogne, UMR 5209 CNRS/Université de Bourgogne, 21078 Dijon, France (e-mail: jfatome@u-bourgogne.fr).

Color versions of one or more of the figures in this paper are available online at http://ieeexplore.ieee.org.

Digital Object Identifier 10.1109/JLT.2011.2117413

with a strong excitonic absorption in the telecommunication wavelengths window, were used as active layers. To amplify the nonlinear response and to reduce the switching energy, the active layer is contained in an asymmetric Fabry–Perot microcavity (AFPM). The QWs are suitably located at one antinode of the intracavity intensity. The AFPM enhances the intracavity intensity of electromagnetic field and, thus, combined with the excitonic absorption, improves the nonlinearity and decreases the switching energy. Furthermore, the SA microcavity device is used at normal incidence, thus yielding intrinsic polarization-insensitive operation.

The total field reflectivity r_{total} of AFPM results from interferences between the front mirror with reflectivity r_f and the back mirror with reflectivity r_b, modulated by the absorption in the active region

$$r_{\text{total}} = \frac{-r_f + r_b^{\text{eff}} e^{i2\phi}}{1 - r_f r_b^{\text{eff}} e^{i2\phi}}. \tag{1.1}$$

Equation (1.1) expresses the r_{total} in terms of r_f, the effective bottom reflectivity r_b^{eff}, and the single-pass dephasing ϕ. Here $r_b^{\text{eff}} = r_b e^{-N\Gamma\eta}$, where N is the QW number, η is the (carrier density dependent) single-pass absorption per QW, and Γ is the longitudinal confinement factor of the microcavity.

As shown in (1.1), the total reflectance $R_{\text{res}} = |r_{\text{total}}|^2$ at the resonant wavelength is strongly dependent on the values of r_f, r_b and on the absorption in the cavity. Mathematically, in the case of SA-1, where $r_b^{\text{eff}} < r_f, R_{\text{res}}$ decreases when absorption decreases due to a partial cancellation of the reflection from the top and the bottom reflectors. R_{res} is null when the internal absorption exactly balances the two reflections. A decrease of absorption beyond this point will cause an increase of R_{res}. This design provides a stabilization of the reflected output power, which can be used for noise reduction of logical ones. In the case of SA-0, where $r_b^{\text{eff}} > r_f, R_{\text{res}}$ increases when the absorption decreases, and reaches its maximum when the absorption is fully saturated. The SA-0 can be used for ER improvement and noise reduction of logical zeros. Thus, with an initial structure, by modifying the cavity parameters of the AFPM, we can perform a bit-1 regeneration device or an ER improvement device.

MQW-SAs typically have a rather long recovery time, around a few nanoseconds. In order to reduce significantly the response time of SAs and make them compatible with high-bit-rate operation, recombination centers must be introduced during or after crystal growth by mean of low-temperature molecular beam epitaxy [21], ion implantation [22], heavy ion irradiation [10], or Be [23] or Fe doping [24]. Recovery times in the subpicosecond range can be achieved by these methods of damage creation.

In order to study the transfer function of the device for 2R regeneration, several microcavities SA-0 and SA-1 have been fabricated. SAs used in this paper are based on the same initial structure. The absorption region includes 7 ×(AlGaAs/InGaAs) QWs, grown by metal-organic vapor-phase epitaxy (MOVPE). The QWs are contained in an asymmetric Fabry–Perot and located at one antinode of the intracavity intensity. The back mirror was made by deposition of a silver layer, with a calculated reflectivity of 0.945. The sample was mounted on a

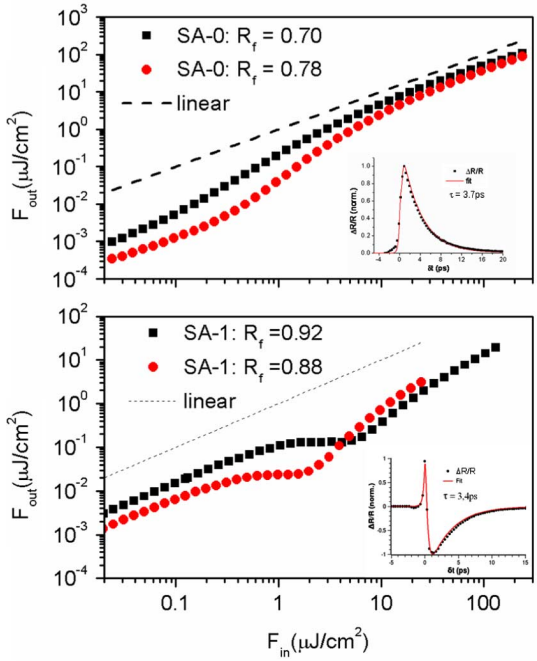

Fig. 1. Transfer functions of SA-0 (a) and SA-1 (b) with different reflectivities of front mirror. The straight lines are the linear functions.

Si substrate by Au–In bonding to make easier the heat dissipation and limit the thermo-optic effects [25]. As previously indicated, the SA characteristics depend strongly on the cavity mirror reflectivities and on the absorption of the active layer included in cavity. In order to investigate the influence of each component on the operation of the 2R regeneration device, different front mirror reflectivities were used. In the case of SA-0 structures, two devices with different ER improvements have been fabricated. The first was designed to have a reflectivity close to zero at low intensity (impedance matching) giving a high ER improvement. The top mirror in this case consisted of two pairs of [SiO_2/TiO_2: $\lambda/4 : \lambda/4$] with 0.78 power reflectivity. The second device had a front mirror made of 6.5 ×[InP/InGaAsP] with 0.70 reflectivity, resulting in a lower ER improvement but a lower insertion loss. For SA-1 structures, the top mirrors were, respectively, made by deposition of 3×[YF_3/ZnS: $\lambda/4 : \lambda/4$], with a calculated reflectivity of 0.92, and by deposition of 5×[InP/InGaAsP: $\lambda/4 : \lambda/4$] and a one-period dielectric coating [YF_3/ZnS:$\lambda/4 : \lambda/4$] on the top, to obtain a front mirror reflectivity of 0.88. The change of front mirror reflectivities allows to modify the stabilization power level of the device. Fig. 1 displays the reflected output fluence (energy density) of SA-0 [see Fig. 1(a)] and of SA-1 [see Fig. 1(b)], as a function of input fluence. These transfer functions were measured at 1550 nm with a pulse source at 10-MHz repetition and 0.8-ps pulse duration. The influence of the front mirror reflectivity on the behavior of each SA device is clearly apparent on the figures. A larger ER improvement can be achieved with the structure SA-0 working at impedance matching. The transfer functions of SA-1s show that the relative amplitude fluctuation at the output would be reduced in the input energy fluence of [1–6 μJ/cm^2] and of [0.6–2 μJ/cm ^{2}] in the case of $R_f = 0.92$ and $R_f = 0.88$, respectively. Moreover, the threshold of high power stabilization (F_{st}) of SA-1

depends on their top mirror reflectivities. The results show that a variation of R_f from 0.92 to 0.88 induces a decrease of $F_{\rm st}$ from 4 μJ/cm^2 to 0.85 μJ/cm^2.

In order to reduce the carrier lifetime, the QWs were irradiated by 12 MeV Ni $^{+6}$ ions with a dose of 4.10^{11} cm $^{-2}$. The inner windows in Fig. 1(a) and in Fig. 1(b) show the time response of the SA-0 and SA-1 devices, respectively, measured by pump–-probe technique at 1550 nm with a 10-MHz repetition rate and 0.65-ps pulses. The results show a response of about 3.7 ps for the SA-0 device and of 3.4 ps for the SA-1. These values are short enough to allow signal regeneration up to 40 Gb/s.

III. Device Modeling

First, we describe our model for SA device. The numerical calculation performs a self-consistent resolution of the variations of carrier density N_c with the parameters characterizing the incident optical signals at given laser wavelength. We assume that N_c is independent of λ, and the calculations are essentially the solution of a series of steady-state equations.

To account for the microcavity effects, we use essentially the Fabry–Perot model equations of [25]. The microcavity reflectivity R can be calculated from equation

$$R = |r|^2 = \frac{\left(r_f - r_b^{\rm eff}\right)^2 + 4 r_f r_b^{\rm eff} \sin^2 \phi}{\left(1 - r_f r_b^{\rm eff}\right)^2 + 4 r_f r_b^{\rm eff} \sin^2 \phi} \tag{1.2}$$

where R is dependent on the working wavelength $\lambda_{\rm work}$ and on the carrier density N_c through the parameter ϕ

$$\phi = (\lambda_{\rm work} - \lambda_{\rm res}) \left(\frac{d\phi}{d\lambda}\right)_{\lambda_{\rm res}} + \frac{d\phi}{dN_c} N_c \tag{1.3}$$

where $\lambda_{\rm res}$ is the microcavity resonance wavelength, $d\phi/d\lambda$ and $d\phi/dN_c$ are obtained from experimental results.

When the QWs are excited near the bandgap, the absorption coefficient is assumed, as in a two-level system, to decrease linearly with carrier density N_c, i.e., [26], [27],

$$\eta = \eta_0 \left(1 - \frac{N_c}{N_t}\right) \tag{1.4}$$

where N_t is the transparency carrier density of the SA, assumed equal to 2.10^{12} cm $^{-2}$ in the present calculation, and η_0 is unsaturated value of η.

For simplicity, we neglect ultrafast intraband relaxation effects, such as spectral hole burning and carrier heating, as they occur on a femtosecond time scale much shorter than the optical pulses. The time evolution of photo-excited carrier density in the QW SA is governed by the following rate equation [28]:

$$\frac{dN_c}{dt} = \frac{\eta I_{\rm QW}}{\hbar\omega} - \frac{N_c}{\tau_r} \tag{1.5}$$

where $I_{\rm QW}$ is the effective intensity within the active layers, τ_r is the carrier recombination time, $\hbar$ is the reduced Planck's constant, and ω is the incident laser angular frequency.

$I_{\rm QW}$ is related to the maximal intracavity intensity $I_{\max}$ through [29]

$$I_{\rm QW} = \frac{\Gamma}{2} I_{\max} \tag{1.6}$$

where $I_{\max}$ is related to the intensity incident I_0 at normal incidence through

$$I_{\max} = \frac{\left(1 + r_b^{\rm eff}\right)^2 \left(1 - r_f^2\right)}{\left|1 - r_b^{\rm eff} r_f e^{2i\phi}\right|^2} I_0. \tag{1.7}$$

We have

$$I_{\rm QW} = \frac{\Gamma}{2} \frac{\left(1 + r_b^{\rm eff}\right)^2 (1 - R_f)}{\left|1 - r_b^{\rm eff} r_f e^{2i\phi}\right|^2} I_0. \tag{1.8}$$

With the steady-state condition $dN_c/dt = 0$, the expression for the local carrier density N_c is obtained from

$$N_c = \eta \frac{\tau_r}{\hbar\omega} I_{\rm QW}. \tag{1.9}$$

Inserting (1.8) into (1.9) , we have

$$N_c = \eta \frac{\tau_r}{2\hbar\omega} \frac{\Gamma \left(1 + r_b^{\rm eff}\right)^2 (1 - R_f)}{\left(1 - r_f r_b^{\rm eff}\right)^2 + 4 r_f r_b^{\rm eff} \sin^2 \phi} I_0. \tag{1.10}$$

Solving (1.10) in using (1.4) allows to calculate the transfer function of SA in steady-state condition.

In order to check the concept, numerical calculations based on the SA model in steady-state condition are performed. Different configurations, where SA-1 is placed before SA-0 (SA-1+ SA-0 combination) or inverse (SA-0 + SA1 combination) are considered.

A. (SA-1 + SA-0) Configuration

The building block of the regenerator model consists of a SA-1, an optical amplifier, and SA-0. The optical amplifier is included in the regenerator model in order to compensate the coupling loss between SA-1 and SA-0. Fig. 2(a) displays numerical nonlinear transfer functions of (SA-1 + SA-0) devices, where SA-0 have 7QW with $R_b = 0.945$, while R_f varies and SA-1 have 7QW with $R_f = 0.92$. Another parameter value for simulation are displayed in Table I. A coupling loss is compensated completely by an optical amplifier. In this case, the stabilization at high level can be obtained, while the ER could not be improved. Moreover, the inserted loss of (SA1 + SA0) module is high. The inefficacity of this configuration for 2R regeneration is proved in [30].

B. (SA-0 + SA-1) Configuration

The regenerator model consists of a dual SA-0 and SA-1 with the same parameter values described earlier. A coupling loss of -8 dB between two components is assumed in the calculation and there is no amplifier between SAs. The numerical nonlinear transfer functions of (SA-0 + SA-1) displayed on the Fig. 2(b) , showed that (SA-0 + SA-1) configuration can provide significantly the ER enhancement along with a stabilization at high input level; therefore, it can be used as 2R regenerator. The numerical calculations show the influence of each component SA-0 and SA-1 on the characteristics of the module (SA-0 + SA-1). The ER improvement strongly depends on the SA-0 characteristics, while the stabilization at high input level is defined by the SA-1 parameters.

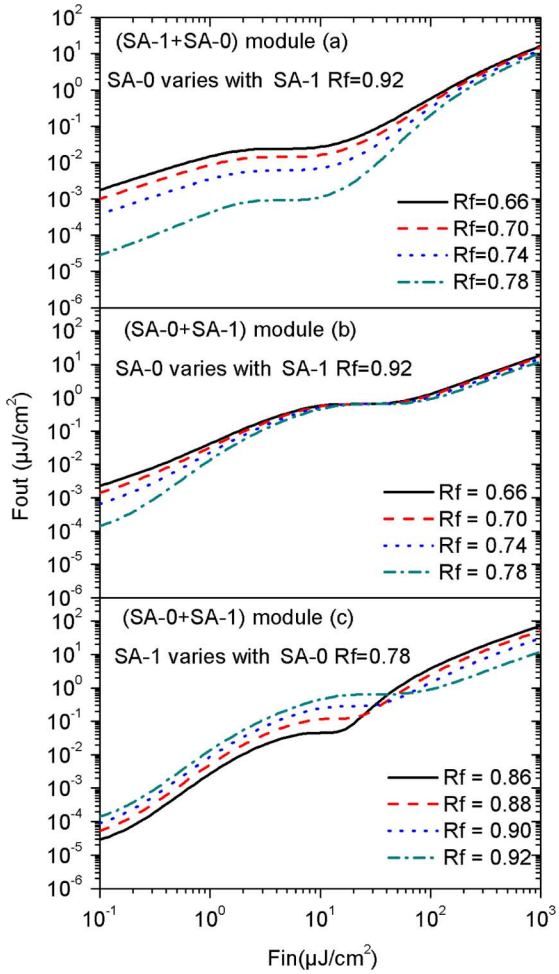

Fig. 2. Numerical transfer functions for the (a) (SA-1 + SA-0) and (b) (SA-0+ SA-1) configurations, where SA-1 is fixed and SA-0 varies and (c) SA-1 varies.

TABLE I
PARAMETERS OF SA-0 AND SA-1 FOR SIMULATION

Parameters	SA-0		SA-1	
R_b	0.95		0.95	
R_f	0.78	0.70	0.92	0.88
N_{QW}	7		7	
Γ	1.63		1.63	
τ (ps)	3.5		3.7	
$d\phi/d\lambda$ (rad/nm)	0.006		0.006	
$d\phi/dN_c$ (rad/cm2)	2.10^{-14}		2.10^{-14}	
λ_{res}	1550		1550	
λ_{work}	1550		1548	

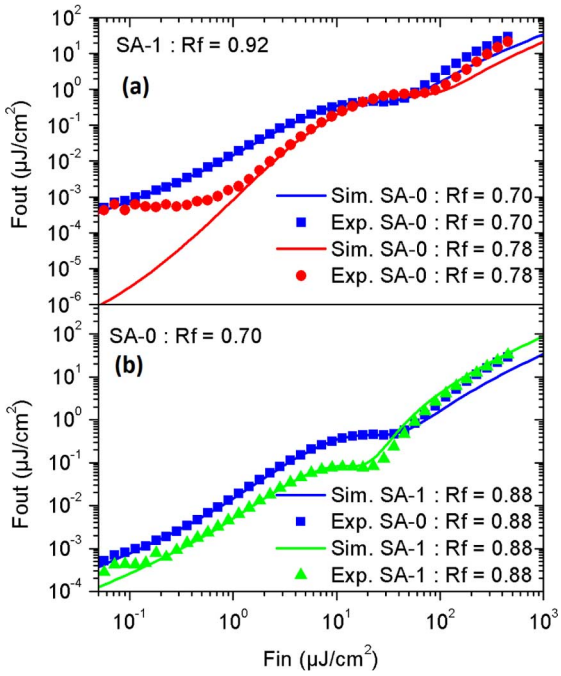

Fig. 3. Reflected output fluence as a function of input fluence, for several device combinations. (a) (SA-0+SA-1) SA-1 fixed with $R_f = 0.92$, SA-0 varies. (b) (SA-0 + SA-1) SA-0 fixed with $R_f = 0.70$, SA-1 varies.

IV. NONLINEAR RESPONSE OF THE DEVICES

To estimate the potential for noise reduction and ER improvement of this device, we measured its transfer functions, i.e., the time-averaged output power versus input power. The experimental setup consists of a mode-locked fiber laser producing 0.8-ps pulses at 10 MHz, with wavelength adjustable in the range of 1540–1565 nm. The dual-stage (SA-0 + SA-1) acts as a complete 2R regenerator. The input signal, after passing through a variable attenuator, is focused onto the sample SA-0. The signal transmitted by SA-0 is injected directly into SA-1 due to the optical circulator. Microlensed fibers producing a spot size of 3.1 μm diameter at 1/*e* intensity were used to focus optical signals on the SA devices. The reflected signal was detected and analyzed by an optical spectrum analyzer (OSA). In this experiment, there was no amplifier between SA-0 and SA-1, and the coupling losses were estimate to -8 dB.

The experimental and numerical transfer functions of (SA-0 + SA-1) devices are displayed in Fig. 3. The parameter values of SA-0 and SA-1 used for simulation are indicated in Table I. As can be seen, a good agreement is obtained between the calculated and experimental results for incident fluences up to 1.5 μJ/cm^2. The disagreement at low input fluence in the case, where SA-1 is fixed and SA-0 with $R_f = 0.78$ is related to the limited sensitivity of the OSA. As shown on Fig. 3, the effect of ER improvement and stabilization at high level can be obtained in this device combination. The possibility to adjust the threshold and ER improvement of the module using the SA-0 and SA-1 individual characteristics is demonstrated. Fig. 3(a) shows the transfer functions of the (SA-0 + SA-1) module when the front mirror of SA-1 is fixed to $R_f = 0.92$. Our measurement showed that the ER is significantly improved with a SA-0 R_f of 0.78 (impedance matching). The change in SA-0 R_f does not change the nonlinearity of the full device at high power level. The increase of stabilization threshold from 22 μJ/cm^2 to 37 μJ/cm^2 when changing the front mirror of SA-0 from $R_f = 0.70$ to $R_f = 0.78$ is related to the higher insertion loss of the SA-0 at impedance matching. In order to determine the influence of SA-1 on the operation of the (SA-0 + SA-1) module, we measured several transfer functions with different SA-1 parameters. The SA-0 was then fixed with $R_f = 0.70$ in this case. Fig. 3(b) shows that the threshold for power stabilization increases from 10 μJ/cm ^{2} to 22 μ J/cm^2 when the front mirror R_f of SA-1 changes from 0.88 to 0.92. The ER improvement of the module did not change.

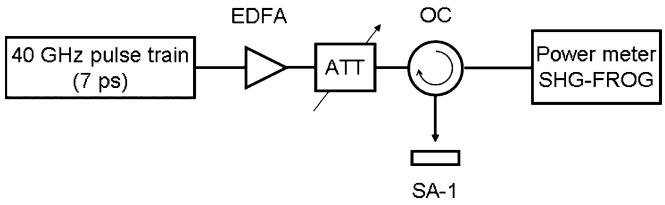

Fig. 4. Experiment setup. Att: variable optical attenuator; EDFA: erbium-doped fiber amplifier; SHG-FROG: second-harmonic regeneration-frequency-resolved optical gating.

The experimental results showed that a complete 2R regeneration can be obtained with the simple high-speed SAs (SA-0 + SA-1) combination device. The optimum configuration could be obtained with the SA-0 working at impedance matching. A reduction of the threshold of bit-1-level stabilization would be expected by reducing the coupling loss between two components. The experimental study of noise reduction involving the two devices operating at the bit rate and bit pattern differences presented in [30] demonstrate the promising character of (SA-0 + SA-1) devices for 2R regeneration at 40 Gb/s.

V. Amplitude and Phase Characterization

The chirp parameter is one of the most important characteristics for modulators. It is proportional to the ratio between the phase variation and the relative amplitude variation. An accurate estimation of the system performance requires the determination of amplitude and phase of the processed signals. In order to characterize the signal in amplitude and phase at high repetition rates we measured the characteristics of a 40 GHz pulse train transmitted by the device, by using the SHG-FROG technique.

A. SA-1 Characterization

The experimental setup is shown in Fig. 4. A high-quality 40 GHz, 7 ps transform-limited pulse train was first generated at 1551 nm (the resonance wavelength of the SA-1 device) by using the multiple four-wave-mixing technique in a 1420 m long Teralight fiber. The signal was focused on the SA-1 device thanks to a fiber-pigtailed high aperture lens producing a focused spot 5 μ m diameter at $1/e^2$ of maximum intensity. The transmitted signal was analyzed by a power meter and a second-harmonic-generation FROG device [13].

The characterization in amplitude and phase of the SA-0 device has already been presented in [12]. The FROG measurements showed the pulse compression effect and no nonlinear phase distortion of SA-0. In this paper, we focus the work on the SA-1 device.

In order to determine the operating regimes of the SA-1 device, we measured it transfer function at 40 GHz. The results, presented in Fig. 5(a), showed that at resonance, SA-1 provides a significant amplitude stabilization of the reflected signal in the average input power range from 40 to 90 mW. Fig. 5(b) shows the intensity and phase profiles with different input power levels. At 15 dBm, the SA-1 is in the linear area. The pulse and phase profiles are identical to the measured reference. The pulse compression effect occurs when the incident power increases, inducing the nonlinear behavior of SA-1. The phase profile is slightly changed. The experimental results are demonstrated the

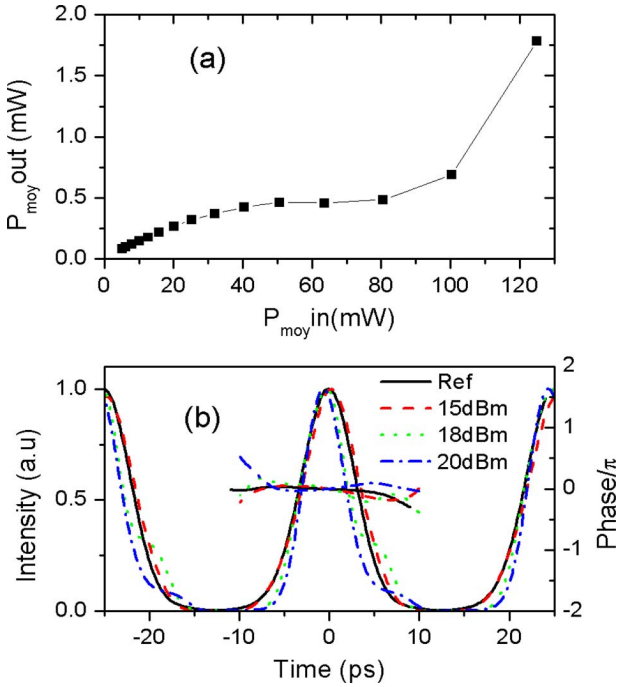

Fig. 5. (a) Transfer function of SA-1 device. (b) FROG result. Intensity profile and phase of the 40 GHz pulse train at the SA-1 input: Au mirror reference and after SA-1 output for linear and nonlinear regimes.

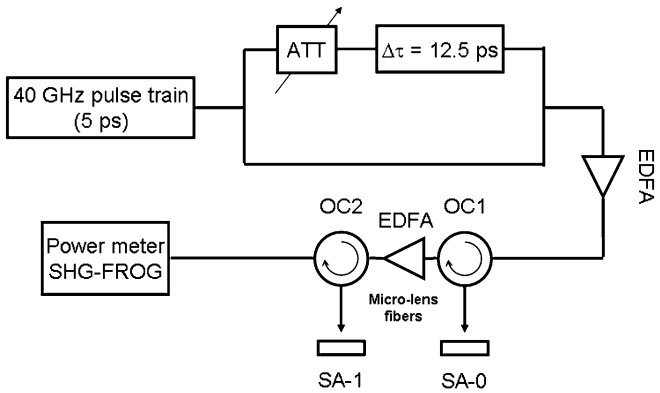

Fig. 6. Experiment setup. Att: variable optical attenuator. $\Delta\tau$ delay line. EDFA: erbium-doped fiber amplifier. OC: optical circulator. SHG-FROG: second-harmonic regeneration—FROG.

dependence of the pulse compression effect on the input power, and showed the low chirp property of SA-1.

B. (SA-0 + SA-1) Module Characterization

In this section, we describe the characterization of a signal transmitted by a module composed of successive devices SA-0 and SA-1. The experimental setup is presented in Fig. 6. The signal is composed of a pulse train with duration of 5 ps at 40 GHz repetition. Then, a 50:50 coupler combined with a 12.5 ps delay line was use to generate through multiplexing in the time domain, the following simplified bit pattern "...01010101..." at 80 GHz. A variable attenuator has also been inserted into the delay line in order to adjust the energy of the ghost-pulses injected into the "0" bit slots.

The transfer function measurements have been realized on dual-stage SA-0 and SA-1. As can be seen in Fig. 7(a), the

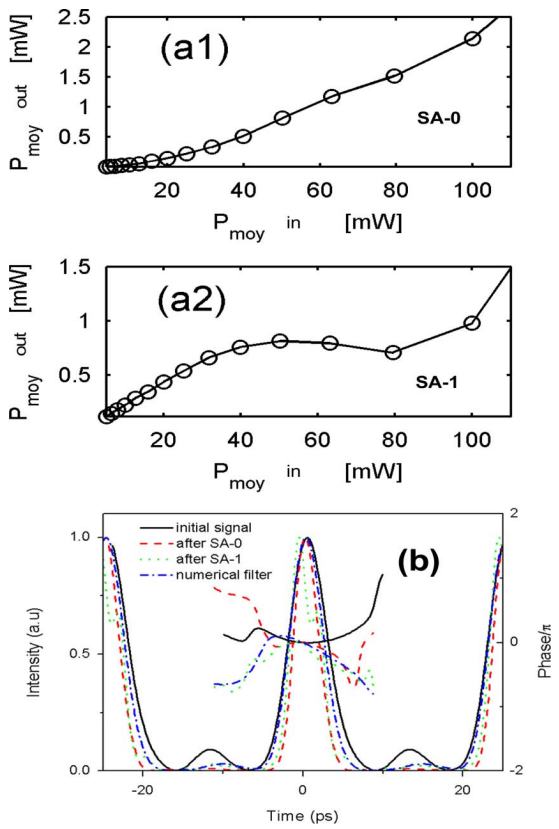

Fig. 7. (a) Transfer function of SA-0 and SA-1 device. FROG results. Intensity profile and phase of signal after passing SA-0 + SA-0 device. The input power on SA-0 is 35 mW and on SA-1 is 60 mW.

nonlinear regime of SA-0, synonymous with ER improvement, occurs for a power below 40 mW and the input power range for noise reduction on the bit-1 levels is between 40 mW and 90 mW.

The FROG measurements were then conducted on each device to determine the intensity and phase profiles of the signal. The results are showed in Fig. 7. The input power on SA-0 is 35 mW and on SA-1 is 60 mW. The ER improvement is clearly observed thanks to the action of SA-0. The pulse compression effect can be also observed and the phase profile is unaffected. After passing through the SA-1 device, the pulse profile becomes slightly asymmetric. This asymmetry is more pronounced than in the previous results shown on Fig. 5(b) because of the duration of the pulses coming out of the first component is 3.5 ps, which is comparable to the response time of SA-1 device. The compression of pulses and the asymmetric effect induce a broader and asymmetric optical spectrum. However, this asymmetry can be compensated by an optical filter, digital here, in order to approach the initial pulse, but at the expense of a slight frequency drift observed on the phase. The signal finally has a clear ER improvement.

VI. Conclusion

We have proposed and demonstrated an all-optical passive device that consists in a combination of two high-speed SA-based components. The numerical calculations, confirmed by experimental results showed that the simple combination of (SA-0 and SA-1) can provide a large ER improvement and a strong nonlinearity. By changing SA-0 and SA-1 parameters, the saturation properties can be controlled, and the threshold values can be controlled. The characterizations in intensity and in phase on (SA-0 + SA-1) module reveal a low chirp property. This device is thus promising for applications to all-optical 2R regeneration at ultrahigh bit rate.

References

[1] O. Leclerc *et al.*, "Optical regeneration at 40 Gb/s and beyond, IEEE," *J. Lightw. Technol.*, vol. 21, pp. 2779–2789, Nov. 2003.
[2] P. V. Mamyshev, "All-optical data regeneration based on self-phase modulation effect," in *ECOC*, 1998, pp. 475–476.
[3] J. K. Lucek and K. Smith, "All-optical signal regenerator," *Opt. Lett.*, vol. 18, pp. 1226–1228, 1993.
[4] S. Bischoff and J. Mork, "All-optical signal regeneration at 40 Gbit/s using a Mach–Zehnder interferometer based on semiconductor optical amplifiers," in *Lasers Electro-Opt. Conf.*, 2000, p. 345.
[5] S. Hojfeldt *et al.*, "All-optical wavelength conversion and signal regeneration using an electroabsorption modulator ," *J. Lightw. Technol.*, vol. 18, no. 8, pp. 1121–1127, Aug. 2000.
[6] D. Wolfson *et al.*, "40-Gb/s all-optical wavelength conversion, regeneration, and demultiplexing in an SOA-based all-active Mach–Zehnder interferometer," *IEEE Photon. Technol. Lett.*, vol. 12, no. 3, pp. 332–334, Mar. 2000.
[7] M. Matsumoto, "Analysis of optical regeneration utilizing self-phase modulation in a highly nonlinear fiber ," *Photon. Technol. Lett.*, vol. 14, pp. 319–321, 2002.
[8] S. Radic *et al.*, "All-optical regeneration in one- and two-pump parametric amplifiers using highly nonlinear optical fiber," *Photon. Technol. Lett.*, vol. 15, pp. 957–959, Jul. 2003.
[9] E. Seguineau *et al.*, "Regeneration capabilities of passive saturable absorber-based optical 2R in 20 Gbit/s RZ DWDM long-haul transmissions," *Electron. Lett.*, vol. 39, no. 11, pp. 857–858, Mar. 2003.
[10] J. Mangeney *et al.*, "Comparison of light- and heavy-ion-irradiated quantum-wells for use as ultrafast saturable absorbers ," *Appl. Phys. Lett.*, vol. 79, pp. 2722–2724, 2001.
[11] J. Mangeney *et al.*, "Sub-picosecond wideband efficient saturable absorber created by high energy (200 MeV) irradiation of Au^{+} ions into bulk GaAs," *Electron. Lett.*, vol. 34, no. 8, pp. 818–820, Apr. 1998.
[12] D. Massoubre *et al.*, "All-optical extinction-ratio enhancement of a 160 GHz pulse train by a saturable-absorber vertical microcavity," *Opt. Lett.*, vol. 31, pp. 537–539, Feb. 15, 2006.
[13] J. Fatome *et al.*, "All-optical reshaping based on a passive saturable absorber microcavity device for future 160-Gb/s applications," *Photon. Technol. Lett.*, vol. 19, pp. 245–247, 2007.
[14] L. Bramerie *et al.*, "Cascadability and wavelength tunability assessment of a 2R regeneration device based on a 8 channel saturable absorber module," presented at the presented at the Opt. Fiber Conf. , Anaheim, CA, 2007.
[15] M. Gay *et al.*, "Bit-error-rate assessment of 170-Gb/s regeneration using a saturable absorber and a nonlinear-fiber-based power limiter," *Photon. Technol. Lett.*, vol. 22, pp. 158–160, 2010.
[16] M. Gay *et al.*, "Cascadability assessment of a 2R regenerator based on a saturable absorber and a semiconductor optical amplifier in a path switchable recirculating loop," *Photon. Technol. Lett.*, vol. 18, pp. 1273–1275, 2006.
[17] H. T. Nguyen *et al.*, "New passive all-optical semiconductor device for bit-1 level noise reduction," presented at the presented at the Eur. Conf. Lasers Electro-Opt. Int. Quantum Electron. Conf. (CLEOE-IQEC), Munich, Germany, 2007.
[18] H. T. Nguyen *et al.*, "A passive all-optical semiconductor device for level amplitude stabilization based on fast saturable absorber," *Appl. Phys. Lett.*, vol. 92, pp. 111107-1–111107-3, 2008.
[19] D. Massoubre *et al.*, "Scaling of the saturation energy in microcavity saturable absorber devices," *Appl. Phys. Lett.*, vol. 88, pp. 153513-1–153513-3, 2006 .
[20] R. Trebino *et al.*, "Measuring ultrashort laser pulses in the time-frequency domain using frequency-resolved optical gating," *Rev. Sci. Instrum.*, vol. 68, pp. 3277–3295, Sep. 1997.
[21] R. Takahashi *et al.*, "Ultrafast 1.55-mu m photoresponses in low-temperature-grown InGaAs/InAlAs quantum wells ," *Appl. Phys. Lett.*, vol. 65, pp. 1790–1792, 1994.
[22] E. L. Delpon *et al.*, "Ultrafast excitonic saturable absorption in ion-implanted InGaAs/InAlAs multiple quantum wells ," *Appl. Phys. Lett.*, vol. 72, pp. 759–761, 1998.
[23] D. Vignaud *et al.*, "Electron lifetime of heavily Be-doped In[sub 0.53]Ga[sub 0.47]As as a function of growth temperature and doping density," *Appl. Phys. Lett.*, vol. 80, pp. 4151–4153, 2002.

[24] M. Guezo *et al.*, "Nonlinear absorption temporal dynamics of Fe-doped GaInAs/InP multiple quantum wells ," *Appl. Phys. Lett.*, vol. 94, pp. 2355–2359, 2003.
[25] D. Massoubre *et al.*, "Analysis of thermal limitations in high-speed microcavity saturable absorber all-optical switching gates," *J. Lightw. Technol.*, vol. 24, no. 9, pp. 3400–3408, 2006.
[26] E. Garmire, "Resonant optical nonlinearities in semiconductors," *IEEE J. Sel. Top. in Quantum Electron.*, vol. 6, no. 6, pp. 1094–1110, 2000.
[27] D. S. Chemla and D. A. B. Miller, "Room-temperature excitonic nonlinear-optical effects in semiconductor quantum-well structures ," *J. Opt. Soc. Amer. B*, vol. 2, pp. 1155–1173, 1985.
[28] H. A. Haus and Y. Silberberg, "Theory of mode locking of a laser diode with a multiple-quantum-well structure," *J. Opt. Soc. Amer. B*, vol. 2, pp. 1237–1243, 1985.
[29] S. W. Corzine *et al.*, "Design of Fabry–Perot surface-emitting lasers with a periodic gain structure," *J. Quantum Electron.*, vol. 25, pp. 1513–1524, 1989.
[30] Q. T. Le *et al.*, "All-optical 2R regeneration using passive saturable absorption," *Opt. Commun.*, vol. 282, pp. 2768–2773, 2009.

Hoang Trung Nguyen was born in Hue, Vietnam, on March 14, 1979. He received the Ph.D. degree in physics from the Laboratory for the Photonics and Nanostructures, Centre National de la Recherche Sciencetifique, Marcoussis, France, in 2009. His Ph.D. thesis was focused on all-optical saturable absorber-based microcavities for 2R passive all-optical regeneration at ultrahigh bit rate.

His research interests include all-optical regeneration and optical communication systems.

Coraline Fortier was born in Besancon, France, on December 4, 1980. She received the Ph.D. degree in physics from the Laboratory Interdisciplinary Carnot of Burgundy, University of Burgundy, Dijon, France, in 2011. His Ph.D. thesis was focused on development and studies on the insertion of optical functions containing special fiberoptics (FOS) or semiconductors in lines of transmission to high banc (160 Gb/s and more).

His research interests include new systems for telecommunication systems in base on microstructured chalcogenide fibers and all-optical pulse train source generation method.

Julien Fatome was born in Charleville-Méziéres, France, in 1978. He received the Graduate degree from the Engineering School ESIREM, Dijon, France, and the DEA degree and Ph.D. degrees in physics from the University of Burgundy, Dijon, France, in 2000 and 2004, respectively. His Ph.D. thesis was focused on the studies of ultrashort pulse propagation at 160 Gb/s in dispersion-managed optical fiber lines.

Since 2005, he has been a Research Engineer in the Centre National de la Recherche Scientifique (CNRS), Laboratoire Interdisciplinaire Carnot de Bourgogne, University of Burgundy, where he is currently involved in the research on nonlinear effects, pulse trains generation at ultrahigh bit rate, as well as all-optical nonlinear processing and polarization control. He has published more than 70 papers in journals and conference proceedings.

Guy Aubin received the B.S. degree from Ecole Nationale Supérieur des Télécommunications (ENST-Bretagne), Brest, France, and the M.S. degree in information processing from the University of Rennes, Rennes, France, both in 1981.

He was the Head of the Transmission Experimentation Group at the Submarine Networks Department, France Telecom R&D, where he contributed to the world's first demonstration of 40-Gb/s transmission over transoceanic distance, to the first trials of undersea optical amplified links, and, well before, to the definition of first installed fibered systems. He is currently engaged at the Laboratory for Photonics and Nanostructures, French National Scientific Researcher Center (CNRS), Marcoussis, France. His research interests include new device functionalities for telecommunication systems. He is involved in the research on all-optical or optoelectronics functions for next-generation networks and develops advanced demonstrating setups. He is also involved in the research on 40-Gb/s WDM signal regeneration based on the use of irradiated multiple quantum well (MQW) saturable absorption, 40-Gb/s wavelength conversion with electroabsorption modulator, 40-GHz clock recovery with MQW superlattice or self-pulsating lasers, and signal processing characterization with guided photonic crystals.

Jean-Louis Oudar received the B.S. degree from Ecole Polytechnique, Paris, France, in 1971, and the Doctorat es-Sciences degree in physics from the University of Paris, Paris, in 1977.

In 1971, he joined the Centre National d'Etudes des Télécommunications (CNET), where he was involved in the research on nonlinear optical phenomena in condensed matter. By Studying the enhanced optical nonlinearities of organic compounds, he developed the basis of a molecular engineering approach for nonlinear organic materials. In 1979, he spent a year as a Visiting Scientist at the Physics Department, University of California, Berkeley, where he was involved in the research on new techniques of nonlinear spectroscopy based on four-wave mixing. In 1980, he rejoined CNET, which later evolved as France Telecom R&D, where he successively led the Laboratory for Optics Physics and Materials and the Laboratory of Quantum Optoelectronic Devices. His research was conducted on the ultrafast dynamic nonlinearities of III–V semiconductor microstructures, quantum optics of microcavities, and the development of optical bistable and switching devices. From 1991 to 2003, he was a Lecturer in physics at Ecole Polytechnique. Since 2000, he has been with the newly created Laboratory for Photonics and Nanostructures of the Centre National de la Recherche Scientifique (CNRS-LPN), Marcoussis, France, where he is currently leading the Photonic Devices for Telecommunications group. He has authored or coauthored more than 150 research papers in refereed journals, presented more than 60 invited talks at international conferences, and holds nine patents in laser and nonlinear optical devices.

Dr. Oudar has been active in the Editorial Board of several scientific journals, including the *European Physical Journal D*.